RSC Advances

PAPER

View Article Online
View Journal | View Issue

Cite this: *RSC Adv.*, 2014, **4**, 61847

Shape memory polymer nanocomposite with multi-stimuli response and two-way reversible shape memory behavior†

Wenbing Li,[a] Yanju Liu[b] and Jinsong Leng*[a]

Received 18th September 2014
Accepted 10th November 2014

DOI: 10.1039/c4ra10716k

www.rsc.org/advances

In this work, a novel type of shape memory polymer nanocomposite was fabricated using chemically cross-linked poly(ε-caprolactone) with allyl alcohol as the matrix and Fe_3O_4 nanoparticles decorated conductive multiwalled carbon nanotubes (Fe_3O_4@M) as a magnetism and electricity responsive source. The nanocomposite exhibited excellent shape memory performance with a multistage stimulus recovery from a temporary shape to a permanent shape, triggered by an alternating magnetic field, an electric field and hot water, respectively. Uniquely, the nanocomposite also displayed significant two-way reversible shape memory behavior under constant load conditions, which was not demonstrated previously. An alamar blue assay was also used to prove that the material possessed good biocompatibility. The results showed that the material could have good potential application in sensors, functional tissue engineering constructs and artificial muscles.

Introduction

Shape memory polymers (SMPs) are a kind of stimuli-sensitive material that can memorize and recover permanent shapes under external stimulus.[1,2] Nowadays, there are two typical kinds of shape memory behavior in SMPs: "one-way" shape memory behavior and "two-way" shape memory behavior. Since the shape change driven by an external stimulus could only be from a temporary shape to a permanent shape, "one-way" shape memory behavior is identified as a non-reversible feature.[3,4] Relatively, "two-way" shape memory behavior is recognized as a reversible shape shifting feature. That is, under constant stress[5–10] or stress-free conditions,[11,12] the polymer can change back and forth between two distinguished shapes when cyclically heated or cooled on specific temperature regions. The so called "two-way" shape memory polymers have promising potential applications in the fields of actuators and sensors. As far as we know, these polymers can be used as triggered porous membranes in environmental studies,[13] and artificial muscles in the medical field.[14]

To our knowledge, the crystalline molecular chain segments of the semi-crystalline polymers act as thermal switches in the "one-way" shape memory systems.[15–19] However, the "two-way" shape memory behavior presented by semi-crystalline polymers has been reported in some articles.[5,6,20–23] This thermally controlled reversible shape memory effect is due to the reversible transformation of the crystalline regions under a constant tensile load in specific thermo-mechanical conditions.[14,22,24] The crystalline chain segments crystallize in the molecular of polymer and elongate along the direction of the load. When reheated, crystal melting which induces crystalline chain contraction.[25]

During the past decades, shape memory polymers could respond to several external stimuli, including thermal stimulus,[26,27] magnetic stimulus,[28,29] electric stimulus,[30,31] light stimulus,[32,33] and water stimulus.[34,35] However, single stimulus and only one shape memory transition of SMPs are restricted in applications. Therefore, new SMP nanocomposites that can be induced by several external stimuli[36] and can perform multi-shape transitions[37] have drawn more and more attention among researchers.

Nowadays, multi-stimuli sensitive SMP nanocomposites,[34,36] two-way reversible shape memory semi-crystalline polymers,[6] and multishape memory polymer nanocomposite[37] have been prepared by some researchers. However, the polymer with the properties of two-way reversible shape memory effect, various stimulus methods, and multistage stimulus at the same time has not been employed yet. So in this study, Fe_3O_4 loaded multiwalled carbon nanotubes (MWCNTs) nanocomposite particles (Fe_3O_4@M) were firstly fabricated by chemical co-precipitation of Fe^{3+} and Fe^{2+} ions on the surface of the carboxyl-modified MWCNTs.[38] The morphology of the Fe_3O_4 and Fe_3O_4@M were mainly analyzed by dynamic light scattering

[a]*Centre for Composite Materials and Structures, Harbin Institute of Technology (HIT), No. 2 YiKuang Street, PO Box 3011, Harbin 150080, PR China. E-mail: lengjs@hit.edu.cn; Fax: +86-451-86403652; Tel: +86-451-86402328*

[b]*Department of Astronautical Science and Mechanics, Harbin Institute of Technology (HIT), Harbin 150080, PR China*

† Electronic supplementary information (ESI) available: SEM, TEM and DLS images (Fig. S1), DSC curves (Fig. S2) and water contact angle (Fig. S3). See DOI: 10.1039/c4ra10716k

(DLS), scanning electron microscopy (SEM) and transmission electron microscopy (TEM). Subsequently, the biodegradable SMP nanocomposite including chemically cross-linked poly(ε-caprolactone) (c-PCL) with the plasticization of allyl alcohol (AL) and Fe_3O_4@M nanoparticles as magnetism responsive and electrical response sources were added to the polymer matrix, which showed an excellent shape memory effect induced by hot water, alternating magnetic field and electric field. Moreover, since the composite exhibited the shape memory performance which was a recovery process from first 34 °C to last 41 °C, it possessed the ability of multistage drive. In addition, to mitigate the heat shock and significant cell death, the transition temperature zone between 34 °C and 41 °C is regarded ideal.[39,40] On the other hand, the nanocomposite not only showed a satisfying one-way shape memory behavior, but also displayed a significant two-way reversible shape memory effect under constant load conditions.

Experimental section

Materials

Linear PCL, Fe_3O_4 and Fe_3O_4@M nanoparticles were synthesized as described in previous reports.[38,41,42] The weight-average molecular weight (M_w) of linear PCL tested by gel permeation chromatography (GPC; Waters 2695 and 2414) was 112 kDa. The biocompatible Fe_3O_4 nanoparticles with a diameter of about 20 nm were synthesized on the basis of a chemical co-precipitation method.[42] Benzoyl peroxide (BPO) and allyl alcohol (AL) were purchased from Aladdin Industrial Corporation (Shanghai, China). The carboxyl-modified MWCNTs with a diameter of 20–30 nm and a length of 20–30 μm were purchased from Chengdu Institute of Organic Chemistry, Chinese Academy of Sciences. Osteoblasts were obtained from the neonatal rat mandible. Before our experiments, the osteoblasts have been passaged to the third generation. All other chemicals and solvents were of reagent grade or better and used without further purification.

Preparation of allyl alcohol (AL) plasticized crosslinked PCL/Fe_3O_4@M nanocomposite (c-PCL/Fe_3O_4@M)

Synthesis route and FT-IR spectra of c-PCL/Fe_3O_4@M nanocomposite could be referenced in our previous literature.[43] Firstly, pre-weighed AL, BPO and PCL with the AL : BPO : PCL weight ratios of 10 : 15 : 100, 13 : 15 : 100, and 16 : 15 : 100 were dissolved in sufficient $CHCl_3$ under stirring, respectively. Secondly, Fe_3O_4@M nanoparticles (10% to PCL) were ultrasonically dispersed in appropriate DMF for 0.5 h, respectively. Then the Fe_3O_4@M solutions were injected into the mixture solutions mentioned above under high speed stirring. Thirdly, when these nanocomposite solutions changed into a sticky state under stirring, they were further dried in an aerator for 24 h at room temperature, respectively. Finally, the completely dried mixtures with three different proportions were subjected to thermal embossing and crosslinking for 20 min in a stainless steel mold at 130 °C with 2 MPa, respectively.

Characterization methods

The morphology and size of the Fe_3O_4 and Fe_3O_4@M nanoparticles were detected by transmission electron microscopy (TEM, H–700H, Hitachi, Japan) at an electron acceleration voltage of 150 kV. The size and size distribution of the Fe_3O_4 nanoparticles were measured by dynamic light scattering (DLS, ZETA-SIZER Nano-2590, Malvern, UK). The water contact angle (CA) was measured by the contact angle equipment (DSA-100, Kruss, Germany), using sessile drop method at room temperature. The CA was determined at 25 s after the distilled water droplet contacted with the surface of the specimens, and every CA data was an average of five measurements at different positions of the surface.

The morphology of the Fe_3O_4@M and the dispersion of Fe_3O_4@M in the polymer matrix were observed through a scanning electron microscope (SEM, Quanta200, FEI, America), and the nanocomposite sample was freeze-fractured in liquid nitrogen for the observation of the cross-section with SEM. Thermal properties of the nanocomposites were determined by differential scanning calorimetry (DSC, Q 100, TA Instruments, America). In order to eliminate any unknown thermal history of the samples, heating and cooling were repeated from −20 °C to 100 °C. Also, the heating- and cooling-rate were both 10 °C min^{-1}. All the DSC data were obtained from the second heating and cooling process.

Static tensile test was completed by a universal testing machine (Instron 5567, Instron Co., Massachusetts) with the cross-head speed of 1 mm min^{-1} at room temperature. The dynamic mechanical analysis (DMA) data were obtained by using a DMA (Q 800, TA Instruments, America) with tensile resonant mode at a heating rate of 3 °C min^{-1} from −20 to 100 °C and at a frequency of 1 Hz. The storage modulus (E') with the sample size 12 × 4 × 1 mm (length × width × thickness) was tested. Every data was an average of five repeats for each treatment, and there were three parallel samples in each testing condition.

Investigation of the dual-shape memory effect

A strip-shaped sample with size of 12 × 4 × 1 mm (length × width × thickness) was used to measure the dual-shape memory properties. Shape fixity ratio and recovery ratio were tested by DMA (TA DMA-Q 800), and using a controlled force mode on the basis of our designed experiment. Firstly, the stripe was heated at 52 °C for 10 minutes, then straining the specimen at a stress rate of 0.03 MPa min^{-1} to 0.14 MPa, obtained a temporary shape I, marked as ε_s; secondly, cooling to 0 °C, releasing the stress and the strain marked as ε_f; finally, the temporary shape was recovered at 41 °C, and the unrecovered strain marked as ε_{ur}. The shape fixity ratio (R_f) was defined as $\varepsilon_f/\varepsilon_s$. The shape recovery ratio (R_r) was defined as $\varepsilon_f - \varepsilon_{ur}/\varepsilon_f$.

Two-way shape memory testing under constant load conditions

The two-way shape memory behavior was investigated by employing a properly thermo-mechanical cooling-heating cycle,

carrying out by using the aforementioned DMA machine under tensile mode, and maintaining the specimen under a constant non-zero load. The test process included the following four steps:

(i) The tensile specimen was first heated at temperature $T = 60$ °C (at T_m + 20 °C).

(ii) Application of load (corresponding to stress levels of 100, and 200 kPa) at a loading rate of 2 kPa min^{-1}, then maintaining the load and temperature constant for 10 min.

(iii) Cooling under load: keeping the load constant, the specimen was cooled down to temperature $T = -20$ °C with a constant cooling rate of 2 °C min^{-1}, still maintaining the load and the temperature constant for 10 min.

(iv) Re-heating under load: keeping the load constant, the specimen was re-heated upto the temperature $T = 60$ °C at a constant heating rate of 2 °C min^{-1}, finally maintaining the load and the temperature constant for 10 min.

Investigation of the multistage shape memory recovery

Using a strip specimen, the multi-stages shape memory recovery was realized. Prior to shape recovery, the specimen was heated at 45 °C for 5 min, until it was softened completely, and it was bent to a pre-deformed "U" shape by an external force, then maintaining the force constant, the specimen was cooled into 0 °C ice water rapidly, so the energy was stored, and the temporary "U" shape was obtained after unloading at low temperature. Firstly, the "U" shaped specimen recovered partially in an alternating magnetic field; Secondly, the partially recovered "U" shaped specimen continued to recover in a supplied voltage 60 V, and also recovered partially; finally, the specimen gone through the two-stages shape memory recovery, and then recovered to original strip shape entirely in the hot water at 41 °C.

In vitro cytotoxicity assays

The samples were cut into cuboids with size 8 × 8 × 2 mm (length × width × thickness). In order to sterilize, samples were soaked in ethanol (75 wt%) and exposed to ultraviolet irradiation for 60 min before cultured with osteoblasts *in vitro*. The osteoblasts were grown in α-modified essential medium with 10% fetal bovine serum (FBS). The cells with a density of 1×10^4 cells per well were cultured on the samples in the 24-well plates with above-mentioned medium and maintained at 37 °C in a humidfied incubator with 5% CO_2. At the preset time points of 1st, 3rd, and 5th day, Alamar blue assay was used to evaluate the cytotoxicity of materials as described in our previous report.[44] The medium was first removed carefully, then 300 μl Alamar blue solutions (10% Alamar blue, 80% media 199 (Gibcos) and 10% FBS; v/v) were added to each well and incubated for further 3 h at 37 °C, 5% CO_2. Cells cultured in wells without samples were used as blank controls. After 3 hours, the 200 μl Alamar blue solutions of each sample were pipetted into 96-well plates (Sigma) and read at 570 (excitation)/600 (emission) in an ELISA microplate reader (Molecular Devices, Sunnyvale, CA). Results were the mean ± standard deviation of three experiments. In addition, cell morphology on the c-PCL/Fe_3O_4@M samples was observed by fluorescence microscopy (OLYMPUS IX51, Japan). Firstly, the osteoblasts were fixed with 2.5% glutaraldehyde, then using Rodmine123 (Sigma, America) and 2-(4-amidinophenyl)-6-indolecarbamidine dihydrochloride (DAPI, Sigma, America) to stain cytoskeletal structure and nuclei, respectively.

Results and discussion

Characterization of c-PCL/Fe_3O_4@M nanocomposite

Fe_3O_4 were synthesized by a co-precipitation of aqueous Fe^{+3}/Fe^{+2} in alkaline solution.[42] The size of the magnetic nanoparticles is about 20 nm, as shown in SEM and TEM images in Fig. S1A and B of the ESI.† In addition, we can also find that the average size of these nanoparticles is about 20 nm in the DLS analysis in Fig. S1C.† To maintain the excellent magnetic responsive performance, the size of the nanoparticles is appropriate.[29]

Fe_3O_4@M were fabricated by depositing Fe_3O_4 onto the outside surface of the carboxyl-modified MWCNTs.[38] The morphology of Fe_3O_4@M nanocomposites is shown in SEM and TEM images in Fig. 1A. From Fig. 1A, we can find that the most of the outside of WMCNTs is covered by Fe_3O_4 nanoparticles as shown in TEM image, but there is also uncovered surface of the WMCNTs, as shown in SEM image. Therefore, the special structure of the magnetic Fe_3O_4 layer covering the outside of the WMCNTs will make a great contribution to the magnetic properties while the outside of the WMCNTs without loaded Fe_3O_4 will contribute to the good electric properties of the WMCNTs. Fig. 1B shows the dispersion of Fe_3O_4@M nanocomposites in the resultant polymer matrix, which was synthesized according to our previous report.[43] We can see that the Fe_3O_4@M composites (10 wt%) are embedded in the c-PCL matrix from the cross-section of the polymer composite. According to the result, the nanocomposites disperse uniformly and maintain tight contact with the polymer matrix. As we know, the essence of both magnetism-responsive and electro-responsive shape memory effect is still regarded as thermal induction, so the good dispersion of the Fe_3O_4@M nanocomposites and the tight interaction between composites and polymer matrix are of great importance to affect the shape memory effect of the polymer composite.

To determine the transition temperature of the polymer composites, the DSC curves of these composites were tested (Fig. 2A). Due to the branching effect of the AL, the crystallization behavior of PCL was significantly affected as reported in our previous report.[43] From Fig. 2A, the melting transition temperatures of these composites decrease from 43.27 °C to 38.99 °C with AL weight ratio increasing from 10 to 16, which was attributed to the change in the crystallization behavior of the PCL with the introduction of the AL plasticizer, as similarly reported by Li, Lendlein and Fritz,[43,45,46] but all these three samples still display well-defined melting transition. In addition, the similar evolution of the crystallization transition temperatures was shown in Fig. S2 of the ESI.†

Three samples were selected to investigate the dynamic mechanical properties of the composites by using DMA. Fig. 2B

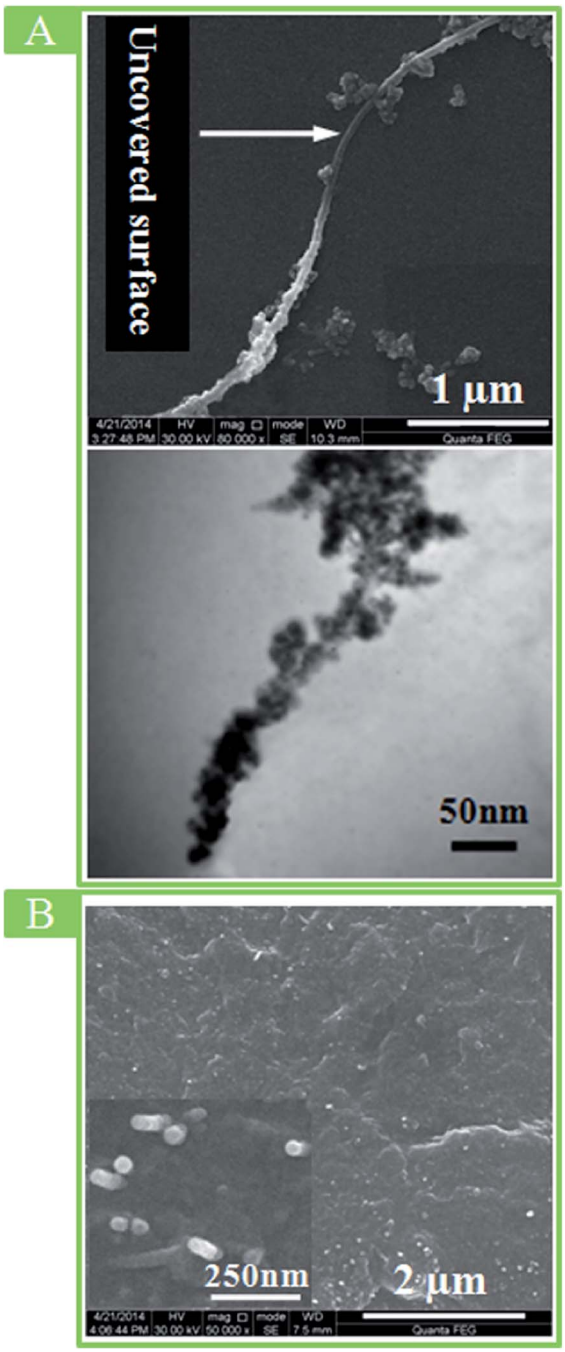

Fig. 1 (A) SEM, TEM micrographs of Fe_3O_4@M nanocomposite particles; (B) SEM micrographs of cross-section for c-PCL/Fe_3O_4@M nanocomposite with 10 wt%.

shows the storage modulus (E') for the composites with different AL : PCL weight ratios. The transition temperature of the composites is a temperature range around the peak of the melting temperature, and shape recovery process can be carried out in the whole range. As temperature and AL content rise, the E' and transition temperatures of all the composites began to gradually drop. From Fig. 2B, we can also find that all the samples show two-step decreases in E', resulted from the glass-rubber transition in a low temperature stage and the melting of

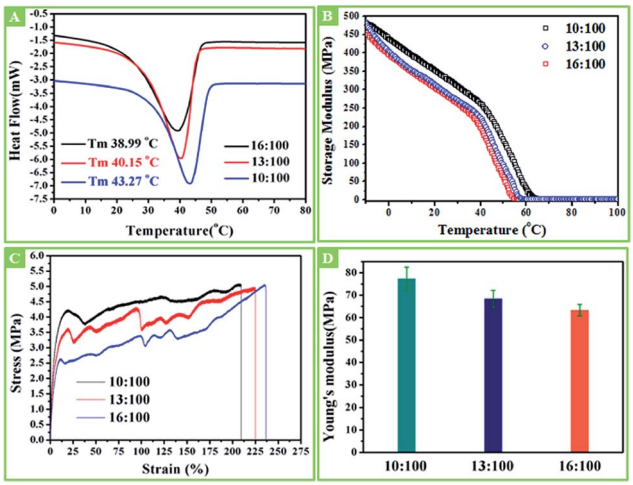

Fig. 2 (A) Representative heating DSC curves showing the T_m of the nanocomposites tested, (B) DMA curves of storage modulus, (C) tensile results at room temperature, and (D) Young's modulus values from the tensile test, of these nanocomposites with AL : PCL weight ratios of 10 : 100, 13 : 100 and 16 : 100.

branched PCL crystallites in a high temperature stage. Furthermore, an apparent inflection point in all these curves was observed close to the melting point, which was caused by the imperfect crystallization of the branched c-PCL. This is consistent with the result of DSC in Fig. 2A. Hence, this just provides a base for the multistage recovery. In addition, this behavior was reported in our previous literature as well.[43]

Typical stress–strain curves of these c-PCL/Fe_3O_4@M composites with different weight ratios of AL were tested by using a universal testing machine at room temperature as shown in Fig. 2C. With the increase of AL content, the elongation at break also increased. From the curve of AL : PCL (16 : 100), the specimen possessed the elongation at the break nearly 236%. Fig. 2D showed the corresponding Young's moduli, which were calculated from the tensile tests. Due to the plasticizing effect of the AL side chains, the Young's moduli and tensile stress decreased gradually with the increasing of AL content.[47] The tensile properties indicated that incoming AL molecules enhanced the segmental mobility of the PCL chains, and also increased the plastic deformation ability of the amorphous region in the PCL.[48]

Fig. S3 in the ESI† exhibits the water contact angle (WCA) of the samples, which is used to evaluate the hydrophilic–hydrophobic property of c-PCL/Fe_3O_4@M composites. The water contact angle (about 62°) shows the hydrophilicity of the c-PCL/Fe_3O_4@M composite could be improved with the introduction of hydrophilic Fe_3O_4 nanoparticles and AL.[49,50] However, it's worth mentioning that the improvement in the hydrophilicity of the material's surface could help to promote cell adhesion when co-cultured with cells.[51,52]

Dual-shape memory property of c-PCL/Fe_3O_4@M nanocomposite

Fig. 3 quantitatively shows the dual-shape memory property of the c-PCL/Fe_3O_4@M composite (13 : 100) tested by DMA.

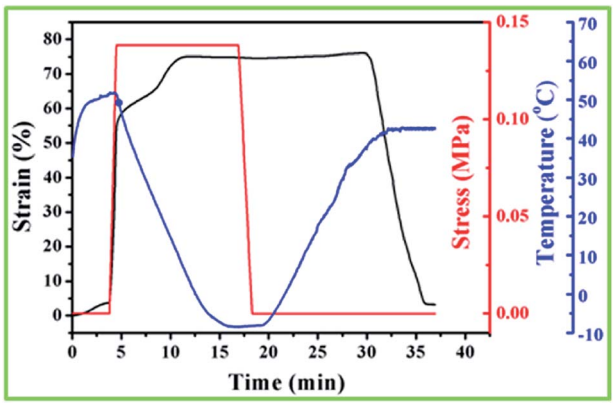

Fig. 3 Shape memory property of c-PCL/Fe_3O_4@M with 13 : 100 measured by DMA.

According to the results of DSC and DMA, we found that the melting peak of the c-PCL/Fe_3O_4@M composite (13 : 100) was 40.15 °C, so the transition temperature of dual-shape memory process was determined as 41 °C. From Fig. 3, the stress-strain-temperature curves were obtained with controlled force mode by DMA testing. Firstly, the sample was heated at 52 °C for 10 minutes, so that it could be softened well; Secondly, the sample was strained at a constant stress, obtained a pre-deformed shape with ε_s for 75.08%; Thirdly, cooling to −10 °C, releasing the stress, then the temporary shape was fixed; finally, the sample was reheated to 41 °C and the temporary shape could be recovered to original shape. In addition, the R_f and R_r of the dual-shape memory cycle were calculated, and the value of R_f and R_r was 99.3% and 95.7%, respectively. Compared to c-PCL/Fe_3O_4@M nanocomposite, the shape memory property (R_f = 94.2%, R_r = 96.8%) of neat c-PCL/AL matrix was shown in our previous report,[53] conforming that the introduction of Fe_3O_4@M almost has no effect on the shape memory property of c-PCL/Fe_3O_4@M composite.

Two-way shape memory behavior of c-PCL/Fe_3O_4@M nanocomposite under constant load conditions

It is well known that crystallizable segments, acting as the integral part of polymer network structures, could easily elongate due to crystallization. The cooling-induced elongation and crystallization events occur at coincidently temperatures, we conclude that the increase in strain is caused by crystallization event. Moreover, when heating back to the original temperature, the cooling-induced elongation event could be almost completely reversed *via* heat-induced contraction. At the same time, this process reveals significant hysteresis due to undercooling of the crystallization. And it can be concluded that segment melting acts as initiator for specimen shrinkage because of entropy elasticity.[9,14] In this work, when the specimen suffered from cooling–heating cycles across the crystallization and melting areas under the application of a constant load, the significant two-way reversible shape memory properties were exhibited. From Fig. 4A, the typical appearance of a two-way shape memory cycle was displayed for the c-PCL/

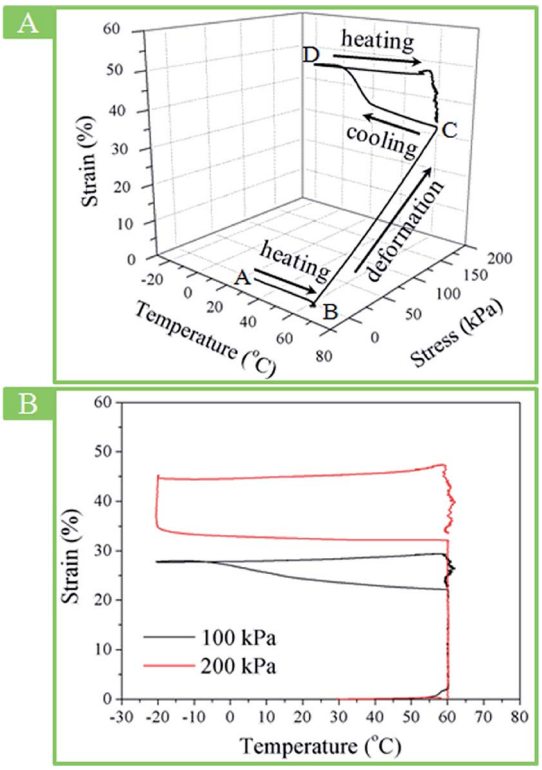

Fig. 4 (A) Typical thermo-mechanical history employed for the evaluation of the two-way shape memory effect under constant load conditions, consisting in: (i) a first heating up to 60 °C (A and B); (ii) a load-controlled deformation up to a maximum nominal stress (B and C); (iii) cooling under the applied load at 2 °C min^{-1} (C and D); (iv) heating again up to 60 °C (D and C). The curve refers to the c-PCL/Fe_3O_4@M with 13 : 100 under the application of a constant stress of 200 kPa. (B) Two-way shape memory response for the specimen subjected to a cooling–heating cycle on a −20 °C/60 °C temperature range and to applied stress levels of 100 and 200 kPa.

Fe_3O_4@M composite (13 : 100) under the application of a tensile load of 200 kPa. The curve could be described as the following four cycle segments. (A and B): Firstly, the specimen was heated from room temperature to T_{high} = 60 °C when no load was applied; (B and C): secondly, the specimen was stretched until a stress of 200 kPa, simultaneously the value of the first elongation was up to 32.22%, in order to guarantee the strain to reach a stable value, the load and temperature were kept constant for 10 min; (C and D): thirdly, the specimen was cooled down to temperature T_{low} = −20 °C, which was lower than the crystallization temperature (T_c = 0.08 °C) of the sample. During the cooling process, the specimen showed continuous increase in strain, which was particularly intense at temperature close to that of the crystallization process. Herein, the load and low temperature were also kept constant for 10 min; (D and C): finally, when reheated up to T_{high}, the strain of the specimen decreased close to 60 °C, and almost completely recovered to original length on account of the previous cooling process under stress.

To describe the effects of the applied stress, the results of the cooling–heating cycles were represented as strain *vs.* temperature curves for the various applied loads, as shown in Fig. 4B;

taken c-PCL/Fe_3O_4@M composite (13 : 100) as an example, the specimen deformed at T_{high} = 60 °C, and then underwent a cooling–heating cycles between T_{high} and T_{low} = −20 °C. From Fig. 4B, we found that the two-way shape memory cycles presented a similar shape for all the values of stress (100 kPa, 200 kPa), and exhibited a continuous increase of strain during cooling, when the sample was reheated to T_{high}, the cooling induced elongation could be recovered to its original length. In addition, it was worth mentioning that the two-way shape memory effect was markedly more pronounced under the application of increasing stresses. Therefore, higher loads resulted in larger elongation, for both the entropic and crystallization induced contributions.[6]

Multi-stimuli shape memory recovery of c-PCL/Fe_3O_4@M nanocomposite

On the basis of our previous report,[43] the c-PCL/Fe_3O_4@M composite with AL–PCL ratio of 13 : 100 was selected for the following study. To obtain an intuitive observation of different stimuli, a series of photographs (Fig. 5) showed macroscopic shape memory recovery process of the c-PCL/Fe_3O_4@M composite induced by hot water with different temperatures, an alternating magnetic field with a frequency of 20 kHz and an electric field with a supplied voltage of 60 V, respectively. From Fig. 5A, we could find that the pre-deformed "O" shape recovered partly in 34 °C and 37 °C hot water, then recovered to the original shape completely at 41 °C. Fig. 5B and C showed the recovery process of the temporary folded "U" shape in an alternating magnetic field and an electric field, respectively. Just like in the hot water, the alternating magnetic field and electric field stimuli can also induce shape recovery of the pre-deformed specimen. However, the speeds of shape recovery induced by the alternating magnetic field and electric field were much slower than that induced in direct thermal stimulus. This is because the entire unit was exposed to air, so it was hard to avoid heat transfer with the outside environment. This part of heat loss made it need longer time to reach the transition temperature. Herein, it is worth noting that by changing the environmental temperature, the different degrees of recovery of the temporary shape can be tuned. Besides, this Fe_3O_4@M nanocomposite could be applied in other polymers. Take the SMP used in aerospace as example, when combining the Fe_3O_4@M nanocomposite with the polymer matrix, the obtained hybrid material possessed the ability of recovery induced by several stimuli and the ability of electromagnetic shield simultaneously.

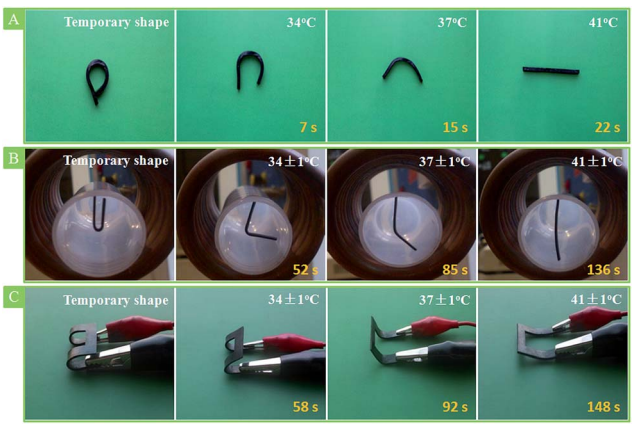

Fig. 5 A Series of digital photographs showing the shape memory recovery process of the c-PCL/Fe_3O_4@M nanocomposite film (A) in 34 °C, 37 °C and 41 °C water, respectively, (B) in an alternating magnetic field with a frequency of 20 kHz and a field strength of 6.8 kA m^{-1} and (C) in the supplied voltage 60 V.

Multi-stages shape memory recovery of c-PCL/Fe_3O_4@M nanocomposite

Remembering more than one permanent shape is an attractive property for triple-shape memory PCL-based polymers.[10,54,55] Compared to currently known triple-shape memory function with two well-separated phase transitions, this thermally activated multistage shape memory behavior could be ascribed to the fact that there existed a diversity of crystalline structure in c-PCL/AL matrix due to the addition of AL. To further verify the multistage shape memory function of c-PCL/Fe_3O_4@M nanocomposite, a macroscopic recovery process was shown in Fig. 6. The specimen exhibited multistage shape memory recovery under the different stimuli, consisting of an alternating magnetic field, electric field and hot water. From Fig. 6A, when the pre-deformed "U" shape specimen was first exposed to 20 kHz alternating magnetic field, the sample was recovered partly; secondly, upon subsequent suffered from 60 V electric field (Fig. 6B), the sample was also controlled to recover partly; Finally, the remaining part of the deformed specimen fully recovered after being heated in hot water at 41 °C (shown in Fig. 6C). Throughout this entire process, the three-stage shape memory recovery of the pre-deformed "U" shape was achieved, confirming that selective different stimuli can indeed allow facile and precise control of the recovery degrees. Therefore, this controllable ability of multi-stages recovery and various recovery methods induced by different stimuli could be promisingly applied in medicine and aerospace field. In addition, the multistage shape memory recovery of the temporary shape was also achieved by using only one actuation.

Biocompatibility analysis

In order to use a biomaterial in medical implantable device, the basic requirement of the material must be non-cytotoxic. Herein, osteoblasts were cultured to evaluate the cytotoxicity of the specimens. Fig. 7A shows the cytotoxicity of c-PCL/Fe_3O_4@M composites with three different weight ratios of AL based on Alamar blue assay. It can be clearly found that the cell viability for all the samples was more than 85% on the first day. After co-culture of 3 days and 5 days, the cell viability of all specimens was more than 95% with no significant difference. Furthermore, the morphology of osteoblasts was observed by a fluorescence microscope, as shown in Fig. 7B. It can be found that the osteoblasts adhered to the material's surface and spread out completely, that is, osteoblasts grew healthily. In addition, the cytotoxicity of Fe_3O_4 was evaluated based on MTT assay and histochemistry analysis as described in our previous

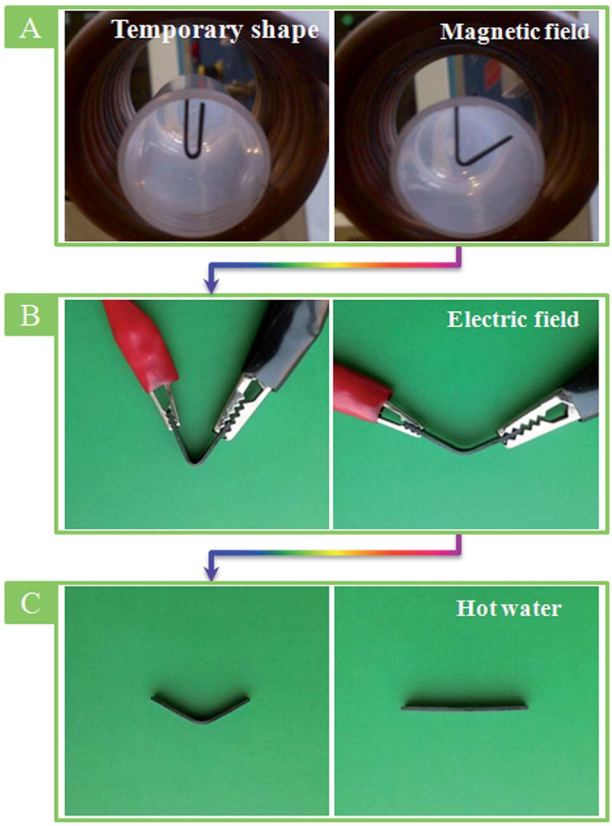

Fig. 6 Series of digital photographs showing multistage shape memory recovery process of the c-PCL/Fe_3O_4@M sample (A) in an alternating magnetic field first, (B) in a supplied voltage 60 V second and (C) in the hot water at 41 °C last.

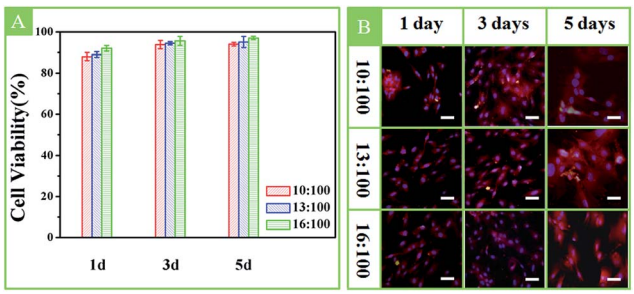

Fig. 7 (A) Alamar blue analysis and (B) fluorescence microscope images of osteoblasts cultured with these nanocomposites with AL : PCL weight ratios of 10 : 100, 13 : 100 and 16 : 100 on the 1st, 3rd and 5th day, respectively. All the scale bars represent 100 μm.

report,[42] the cell viability of Fe_3O_4 nanoparticles was well, so Fe_3O_4 could be considered to be biocompatible. The results suggested that these composites possessed good biocompatibility, and could be potentially used as biomaterials, such as the application in smart medical devices.[27]

Conclusions

In summary, we successfully fabricated a multistage recovery shape memory AL-graft-PCL polymer nanocomposite since it could be facilely tuned by altering the environmental temperature, and activated by multi-stimuli, consisting of an alternating magnetic field, electric field and temperature field. In addition, the nanocomposite also displayed two-way reversible shape memory capabilities when suffered from a constant load during heating and cooling on a thermal region ranging from above the melting temperature to below the crystallization temperature. Moreover, the polymer has good biocompatibility and biodegradation, whose transition temperature in a range close to human physiological temperature. Therefore, the polymer could have great potential for applications in sensors, functional tissue engineering constructs and artificial muscles in the medical areas.

Acknowledgements

This work has been financially supported by the National Nature Science Foundation of China (Grant no. 11225211 and 11272106), for which we are very grateful. The authors thank Prof. S. Zhou for help with the DLS imaging, and Ms. H. Chen for her kind support in the material characterization.

Notes and references

1 A. Lendlein and S. Kelch, *Angew. Chem., Int. Ed.*, 2002, **41**, 2034–2057.
2 A. Lendlein, A. M. Schmidt and R. Langer, *Proc. Natl. Acad. Sci. U. S. A.*, 2001, **98**, 842–847.
3 M. Behl and A. Lendlein, *Mater. Today*, 2007, **10**, 20–28.
4 J. Leng, X. Lan, Y. Liu and S. Du, *Prog. Mater. Sci.*, 2011, **56**, 1077–1135.
5 R. M. Baker, J. H. Henderson and P. T. Mather, *J. Mater. Chem. B*, 2013, **1**, 4916–4920.
6 S. Pandini, F. Baldi, K. Paderni, M. Messori, M. Toselli, F. Pilati, A. Gianoncelli, M. Brisotto, E. Bontempi and T. Ricco, *Polymer*, 2013, **54**, 4253–4265.
7 K. K. Westbrook, P. T. Mather, V. Parakh, M. L. Dunn, Q. Ge, B. M. Lee and H. J. Qi, *Smart Mater. Struct.*, 2011, **20**, 065010.
8 T. H. Kang, J. M. Lee, W. R. Yu, J. H. Youk and H. W. Ryu, *Smart Mater. Struct.*, 2012, **21**, 035028.
9 M. Bothe and T. Pretsch, *Macromol. Chem. Phys.*, 2012, **213**, 2378–2385.
10 Y. Bai, X. Zhang, Q. Wang and T. Wang, *J. Mater. Chem. A*, 2014, **2**, 4771–4778.
11 M. Bothe and T. Pretsch, *J. Mater. Chem. A*, 2013, **1**, 14491–14497.
12 M. Behl, K. Kratz, J. Zotzmann, U. Nöchel and A. Lendlein, *Adv. Mater.*, 2013, **25**, 4466–4469.
13 J. Ahn, W. Yu, J. H. Youk and H. Y. Ryu, *Smart Mater. Struct.*, 2011, **20**, 105024.
14 T. Chung, A. Romo-Uribe and P. T. Mather, *Macromolecules*, 2008, **41**, 184–192.
15 C. Liu, H. Qin and P. T. Mather, *J. Mater. Chem.*, 2007, **17**, 1543–1558.
16 A. Saralegi, S. C. M. Fernandes, A. A. Varona, T. Palomares, E. J. Foster, C. Weder, A. Eceiza and M. A. Corcuera, *Biomacromolecules*, 2013, **14**, 4475–4482.

17 L. Peponi, I. Navarro-Baena, A. Sonseca, E. Gimenez, A. Marcos-Fernandez and J. M. Kenny, *Eur. Polym. J.*, 2013, **49**, 893–903.
18 A. Saralegi, M. L. Gonzalez, A. Valea, A. Eceiza and M. A. Corcuera, *Compos. Sci. Technol.*, 2014, **92**, 27–33.
19 I. Navarro-Baena, J. M. Kenny and L. Peponi, *Cellulose*, 2014, **21**, 4231–4246.
20 J. Zotzmann, M. Behl, D. Hofmann and A. Lendlein, *Adv. Mater.*, 2010, **22**, 3424–3429.
21 J. Li, W. R. Rodgers and T. Xie, *Polymer*, 2011, **52**, 5320–5325.
22 S. Pandini, S. Passera, M. Messori, K. Paderni, M. Toselli, A. Gianoncelli, E. Bontempi and T. Riccò, *Polymer*, 2012, **53**, 1915–1924.
23 J. M. Raquez, S. Vanderstappen, F. Meyer, P. Verge, M. Alexandre, J. M. Thomassin, C. Jérôme and P. Dubois, *Chem.–Eur. J.*, 2011, **17**, 10135–10143.
24 S. J. Hong, W. Yu and J. H. Youk, *Smart Mater. Struct.*, 2010, **19**, 35022.
25 M. Y. Razzaq, M. Behl, K. Kratz and A. Lendlein, *Adv. Mater.*, 2013, **25**, 5730–5733.
26 T. Xie, *Nature*, 2010, **464**, 267–270.
27 A. Lendlein and R. Langer, *Science*, 2002, **296**, 1673–1676.
28 M. Y. Razzaq, M. Behl and A. Lendlein, *Adv. Funct. Mater.*, 2012, **22**, 184–191.
29 X. Yu, S. Zhou, X. Zheng, T. Guo, Y. Xiao and B. Song, *Nanotechnology*, 2009, **20**, 235702.
30 Y. Xiao, S. Zhou, L. Wang and T. Gong, *ACS Appl. Mater. Interfaces*, 2010, **2**, 3506–3514.
31 X. Lan, Y. Liu, H. Lv, X. Wang, J. Leng and S. Du, *Smart Mater. Struct.*, 2009, **18**, 24002.
32 H. Y. Jiang, S. Kelch and A. Lendlein, *Adv. Mater.*, 2006, **18**, 1471–1475.
33 A. Lendlein, H. Jiang, O. Jünger and R. Langer, *Nature*, 2005, **434**, 879–882.
34 L. Wang, X. Yang, H. Chen, G. Yang, T. Gong, W. Li and S. Zhou, *Polym. Chem.*, 2013, **4**, 4461–4468.
35 S. Chen, J. Hu, C. Yuen and L. Chan, *Polymer*, 2009, **50**, 4424–4428.
36 Y. Cai, X. Feng and J. S. Jiang, *J. Appl. Polym. Sci.*, 2014, **131**, 40220.
37 Z. He, N. Satarkar, T. Xie, Y. T. Cheng and J. Z. Hilt, *Adv. Mater.*, 2011, **23**, 3192–3196.
38 H. Pu and F. Jiang, *Nanotechnology*, 2005, **16**, 1486–1489.
39 D. M. Le, K. Kulangara, A. F. Adler, K. W. Leong and V. S. Ashby, *Adv. Mater.*, 2011, **23**, 3278–3283.
40 M. Ebara, K. Uto, N. Idota, J. M. Hoffman and T. Aoyagi, *Adv. Mater.*, 2012, **24**, 273–278.
41 S. Zhou, X. Deng and H. Yang, *Biomaterials*, 2003, **24**, 3563–3570.
42 J. Sun, S. Zhou, P. Hou, Y. Yang, J. Weng, X. Li and M. Li, *J. Biomed. Mater. Res., Part A*, 2007, **80**, 333–341.
43 W. Li, T. Gong, H. Chen, L. Wang, J. Li and S. Zhou, *RSC Adv.*, 2013, **3**, 9865–9874.
44 T. Gong, W. Li, H. Chen, L. Wang, S. Shao and S. Zhou, *Acta Biomater.*, 2012, **8**, 1248–1259.
45 M. Y. Razzaq, M. Behl, U. Frank, J. Koetz, W. Szczerba and A. Lendlein, *J. Mater. Chem.*, 2012, **22**, 9237–9243.
46 S. Jacobsen and H. Fritz, *Polym. Eng. Sci.*, 1999, **39**, 1303–1310.
47 K. Ishida, R. Hortensius, X. Luo and P. T. Mather, *J. Polym. Sci., Part B: Polym. Phys.*, 2012, **50**, 387–393.
48 Z. Kulinski and E. Piorkowska, *Polymer*, 2005, **46**, 10290–10300.
49 J. Xie, C. Xu, N. Kohler, Y. Hou and S. Sun, *Adv. Mater.*, 2007, **19**, 3163–3166.
50 L. Lassila, T. Nohrström and P. K. Vallittu, *Biomaterials*, 2002, **23**, 2221–2229.
51 A. Thapa, D. C. Miller, T. J. Webster and K. M. Haberstroh, *Biomaterials*, 2003, **24**, 2915–2926.
52 Y. Zhu, C. Gao and J. Shen, *Biomaterials*, 2002, **23**, 4889–4895.
53 T. Gong, K. Zhao, G. Yang, J. Li, H. Chen, Y. Chen and S. Zhou, *Adv. Healthcare Mater.*, 2014, **3**, 1608–1619.
54 S. Chen, J. Hu, C. W. Yuen, L. Chan and H. Zhuo, *Polym. Adv. Technol.*, 2010, **21**, 377–380.
55 M. Bothe, K. Y. Mya, E. M. J. Lin, C. C. Yeo, X. Lu, C. He and T. Pretsch, *Soft Matter*, 2012, **8**, 965–972.